Morphology and interaction between lipid domains

Tristan S. Ursell[a], William S. Klug[b], and Rob Phillips[a,1]

[a]Department of Applied Physics, California Institute of Technology, Pasadena, CA 91125; and [b]Department of Mechanical and Aerospace Engineering, Program in Biomedical Engineering, and California NanoSystems Institute, University of California, Los Angeles, CA 90095

Edited by L. B. Freund, Brown University, Providence, RI, and approved June 10, 2009 (received for review April 8, 2009)

Cellular membranes are a heterogeneous mix of lipids, proteins and small molecules. Special groupings enriched in saturated lipids and cholesterol form liquid-ordered domains, known as "lipid rafts," thought to serve as platforms for signaling, trafficking and material transport throughout the secretory pathway. Questions remain as to how the cell maintains small fluid lipid domains, through time, on a length scale consistent with the fact that no large-scale phase separation is observed. Motivated by these examples, we have utilized a combination of mechanical modeling and in vitro experiments to show that membrane morphology plays a key role in maintaining small domain sizes and organizing domains in a model membrane. We demonstrate that lipid domains can adopt a flat or dimpled morphology, where the latter facilitates a repulsive interaction that slows coalescence and helps regulate domain size and tends to laterally organize domains in the membrane.

bilayer mechanics | lipid rafts | membrane morphology

The plasma and organelle membranes of cells are composed of a host of different lipids, lipophilic molecules, and membrane proteins (1). Together, they form a heterogeneous layer capable of regulating the flow of materials and signals into and out of the cell. Lipid structure and sterol content play a key role in bilayer organization, where steric interactions and energetically costly mismatch of lipid hydrophobic thickness result in a line tension that induces lateral phase separation (2). Saturated lipids and cholesterol are sequestered into liquid-ordered (L_o) domains, often known as "lipid rafts," distinct from an unsaturated liquid-disordered (L_d) phase (3–5). Domains whose lipids include saturated sphingolipids and cholesterol, with sizes in the range of ≈50–500 nm, have been implicated in a range of biological processes from lateral protein organization and virus uptake to signaling and plasma-membrane tension regulation (6–18). In the biological setting, maintenance of small domain size is thought to arise from a combination of lipid recycling and energetic barriers to domain coalescence (19–21) [potentially provided by transmembrane proteins (22)], ostensibly resulting in a stable distribution of domain sizes. These biological examples serve as a motivation to better understand the biophysical mechanisms that maintain small lipid domains over time and pose challenges to the classical theories of phase-separation and "domain ripening" [such as Cahn–Hilliard kinetics (23)].

A simple physical model that describes the evolution of lipid domain size and position predicts that domains diffuse and coalesce, such that the number of domains constantly decreases, whereas the average domain size constantly increases (23). Indeed, models of 2D phase separation have been studied in detail for many physical systems (24–27), and where the phase boundary is unfavorable and characterized by an energy per unit length (28), the domain size grows continuously (23, 29, 30). However, membranes can adopt 3D morphologies that affect the kinetics of phase separation (31–35). In those cases where morphology is considered as part of the phase separation model, previously uncharacterized coalescence kinetics emerge (32). Experimentally, model membranes have shown that nearly complete phase separation on the surface of a giant unilamellar vesicle can be reached in as little as 1 minute (3). With these facts in mind, our central questions are: How can model membranes that have phase separated maintain a distribution of small domain sizes on long time scales and short length scales? Are there membrane-mediated (i.e., elastic) forces that inhibit coalescence and spatially organize domains?

We begin to answer these questions by examining the energetics of the membrane using a linear elastic model. A phase-separated membrane is endowed with bending stiffness, membrane tension, an energetic cost at the phase boundary, and domains of a particular size. Membrane bending and tension establish a natural length scale over which a morphological instability develops that switches domains from a flat to "dimpled" shape, similar to classical Euler buckling (36) (see Fig. 1). The dimpling instability is size-selective and "turns on" a membrane-mediated interaction that inhibits domain coalescence. This transition is a precursor to budding and is distinct from transitions that require spontaneous curvature. Although variations in membrane composition may change specific parameter values, the mechanical effects we describe are generic. Thus, these systems exhibit shape-dependent coarsening kinetics that are relevant for a broad class of 2D phase-separating systems. The interaction between domains is a mechanical effect, and we use a model treating dimpled domains as curved rigid inclusions to distill the main principles governing this interaction. Experimentally, we use a model mixture of lipids and cholesterol to show that such an interaction exists between dimpled domains and is well approximated by a simple model. We hypothesize that a combination of lipid recycling (19) and elastic interactions could serve as a mechanism for the organization of domains and the maintenance of small domain sizes in cellular membranes.

The first section of the article outlines the energetic contributions to the mechanical model and predicts the conditions under which domain dimpling occurs. The second section outlines how dimpled domains facilitate an elastic interaction and compares the model interaction to our measurements made in phase-separated giant unilamellar vesicles.

Elastic Model and Morphological Transitions

The energetics of a lipid domain are dominated by a competition—on one hand, the applied membrane tension and bending stiffness both energetically favor a flat domain; on the other hand, the phase boundary line tension prefers any domain morphology (in 3D) that reduces the boundary length. We use a continuum mechanical model that couples these effects, relating the energetics of membrane deformation to domain morphology. As we will show, this competition results in a morphological transition from a flat to dimpled domain shape, where 2 dimpled domains are then capable of interacting elastically.

Lipid domains in a liquid state naturally adopt a circular shape to minimize the phase boundary length (3), allowing us to formulate our continuum mechanical model in polar coordinates. We employ a Monge representation, where the membrane midplane is described by a height function $h(\mathbf{r})$ in the limit of small membrane deformations (i.e., $|\nabla h| < 1$). With this height

Author contributions: T.S.U. and W.S.K. performed research; T.S.U. analyzed data; and T.S.U., W.S.K., and R.P. wrote the paper.

The authors declare no conflict of interest.

This article is a PNAS Direct Submission.

[1]To whom correspondence should be addressed. E-mail: phillips@pboc.caltech.edu.

This article contains supporting information online at www.pnas.org/cgi/content/full/0903825106/DCSupplemental.

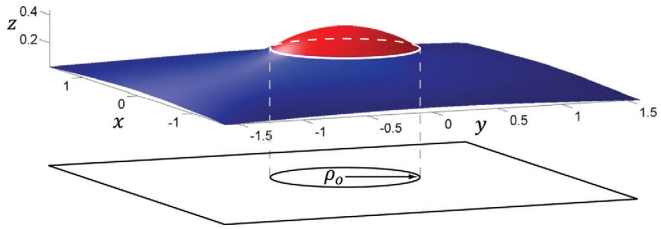

Fig. 1. Three-dimensional rendering of a dimpled lipid domain in dimensionless coordinates. For a domain (shown in red), a competition between bending, membrane tension and phase boundary line tension results in a morphological transition from a flat to a dimpled state as depicted. The dimple costs bending energy but reduces line tension energy by reducing the phase boundary length (shown as a white line around the domain). This morphology facilitates interactions between domains that significantly alter the kinetics of coalescence and lateral lipid organization. The dimensionless projected domain radius is $\rho_o = r_o/\lambda_2$, where r_o is projected radius, and λ_2 is the elastic decay length.

function, we characterize how membrane tension, bending, spontaneous curvature, and line tension all contribute to domain energetics.

Changes in membrane height alter the projected area of the membrane and hence do work against the applied membrane tension, resulting in an increase in energy written as

$$G_{\text{tens}} = \pi\tau\left(\int_0^{r_o}(\nabla h_1)^2 r\mathrm{d}r + \int_{r_o}^{\infty}(\nabla h_2)^2 r\mathrm{d}r\right), \qquad [1]$$

where τ is the constant membrane tension, r_o is the projected radius of the domain, h_1 is the height function of the domain, and h_2 is the height function of the surrounding membrane (37, 38). Membrane curvature is penalized by the bending stiffness with a bending energy written as (37, 39)

$$G_{\text{bend}} = \pi\kappa_b^{(2)}\left(\sigma\int_0^{r_o}(\nabla^2 h_1)^2 r\mathrm{d}r + \int_{r_o}^{\infty}(\nabla^2 h_2)^2 r\mathrm{d}r\right). \qquad [2]$$

This model allows the domain and surrounding membrane to have differing stiffnesses, $\kappa_b^{(1)}$ and $\kappa_b^{(2)}$ respectively, characterized by the parameter $\sigma = \kappa_b^{(1)}/\kappa_b^{(2)}$, and from this point on we drop the superscript on $\kappa_b^{(2)}$. Recent experiments suggest that the bending moduli of a cholesterol-rich domain and the surrounding membrane are approximately equal (5, 40), and hence for simplicity, we assume that the bending moduli of the 2 regions are equal (i.e., $\sigma = 1$), unless otherwise noted. In addition to bending stiffness, the domain may exhibit a preferred "spontaneous" curvature due, for instance, to lipid asymmetry (35, 41). The contribution of domain spontaneous curvature can be simplified to a boundary integral that couples to the overall curvature field by

$$G_{\text{spont}} = -2\pi\,\sigma\kappa_b c_o\int_0^{r_o}(\nabla^2 h_1) r\mathrm{d}r = -2\pi\,\sigma\kappa_b c_o r_o\epsilon, \qquad [3]$$

where c_o is the spontaneous curvature of the domain, and ϵ is the membrane slope at the phase boundary. Furthermore, we assume the saddle-splay curvature moduli are equal in the 2 regions, yielding no dependence on Gaussian curvature. In principle, this contribution could be accounted for with a boundary term, explored in detail in supporting information (SI) *Appendix*. The phase boundary line tension is applied to the projected circumference of the domain, as shown in Fig. 1, by $G_{\text{line}} = 2\pi r_o\gamma$, where γ is the energy per unit length at the phase boundary.

Finally, a constraint must be imposed that relates the actual domain area, $\mathcal{A}$, to the projected domain radius r_o. The energetic cost to change the area per lipid molecule is high [≈50–100 k_BT/nm^2 where $k_B = 1.38\times10^{-23}J/K$ and $T = 300\,K$ (42)]; hence, we assume the domain area is conserved during any morphological change (see *SI Appendix* for details). We impose this constraint using a Lagrange multiplier, τ_o, with units of tension by

$$G_{\text{area}} = \tau_o\left(\pi\int_0^{r_o}(\nabla h_1)^2 r\mathrm{d}r + \pi r_o^2 - \mathcal{A}\right). \qquad [4]$$

This results in an effective membrane tension within the domain $\tau_1 = \tau + \tau_o$, which must be negative to induce dimpling. Examining the interplay between bending and membrane tension, we see that 2 natural length scales emerge—within the domain we define $\lambda_1 = \sqrt{\sigma\kappa_b/\tau_1}$, and outside the domain we define $\lambda_2 = \sqrt{\kappa_b/\tau}$. These length scales allow us to define the relevant dimensionless parameters in this system.

The total free energy of an elastic domain and its surrounding membrane is then the sum of these 5 terms, $G = G_{\text{tens}} + G_{\text{bend}} + G_{\text{spont}} + G_{\text{line}} + G_{\text{area}}$. Details on all the terms in the free energy can be found in *SI Appendix*. With this free energy in hand, we examine how the morphology of a circular domain evolves as we tune domain size and the elastic properties of the membrane.

The height field and radius can be rescaled by the elastic decay lengths such that the Euler–Lagrange equation for the domain can be written in the parameter-free form $\nabla^2(\nabla^2+\beta^2)\eta_1 = 0$, whereas the equation for the surrounding membrane is $\nabla^2(\nabla^2-1)\eta_2 = 0$, where the dimensionless variables are defined by $\lambda_2\eta_i = h_i$, $\lambda_2\rho = r$, $\lambda_2\rho_o = r_o$ and $\beta = i\lambda_2/\lambda_1$. Using the same dimensionless notation, the energy from line tension and spontaneous curvature can be written as $G_{\text{line}} = 2\pi\kappa_b\rho_o\chi$ and $G_{\text{spont}} = -2\pi\,\sigma\kappa_b\epsilon\rho_o\upsilon_o$, with $\upsilon_o = \lambda_2 c_o$ and $\chi = \gamma\lambda_2/\kappa_b$. The dimensionless line tension, χ, is simply a rescaled version of the line tension γ and is 1 of 2 key parameters that characterize the morphological transition; the dimensionless domain area, $\alpha = \mathcal{A}/\lambda_2^2$, is the second key parameter.

The admissible solutions for $\eta_1(\rho)$ and $\eta_2(\rho)$ are zeroth order Bessel functions $J_0(\beta\rho)$ and $K_0(\rho)$, respectively, with the boundary conditions $|\nabla\eta_1(0)| = |\nabla\eta_2(\infty)| = 0$ and $|\nabla\eta_1(\rho_o)| = |\nabla\eta_2(\rho_o)| = \epsilon$. The boundary slope, ϵ, is the parameter that indicates the morphology of the domain; $\epsilon = 0$ indicates a flat domain, whereas $0 < |\epsilon| \lesssim 1$ indicates a dimpled domain. The 5 contributions to membrane deformation energy yield a relatively simple expression for the total free energy, given by

$$G = \pi\kappa_b\rho_o\left[\epsilon^2\left(\sigma\beta\frac{J_0(\beta\rho_o)}{J_1(\beta\rho_o)} + \frac{K_0(\rho_o)}{K_1(\rho_o)}\right) + 2(\chi - \epsilon\sigma\upsilon_o)\right] - \kappa_b(\sigma\beta^2+1)(\pi\rho_o^2 - \alpha). \qquad [5]$$

Mechanical equilibrium is enforced by rendering the energy stationary with respect to the unknown parameters ϵ, ρ_o, and β,

$$\frac{\partial G}{\partial\epsilon} = 0, \quad \frac{\partial G}{\partial\rho_o} = 0, \quad \frac{\partial G}{\partial\beta} = 0. \qquad [6]$$

These equilibrium equations physically correspond to torque balance at the phase boundary, lateral force balance at the phase boundary, and domain area conservation, respectively.

Analysis of the equilibrium equations reveals a second-order transition at a critical line-tension, χ_c, as shown in Fig. 2. For χ less than this critical value, only the flat, trivial solution with $\epsilon = 0$ exists. At χ_c a nontrivial solution describing buckled or dimpled morphologies emerges. For zero spontaneous curvature, the bifurcation is defined by a transcendental characteristic equation

$$\sigma\beta\frac{J_0(\beta\rho_o)}{J_1(\beta\rho_o)} + \frac{K_0(\rho_o)}{K_1(\rho_o)} = 0, \qquad [7]$$

with $\beta = \sqrt{(\chi_c/\rho_o - 1)/\sigma}$ and $\rho_o = \sqrt{\alpha/\pi}$. For a given dimensionless domain area, α, this defines the critical line tension required to dimple the domain. In Fig. 2*A Inset*, this relation is used to generate a morphological phase diagram that shows where in the

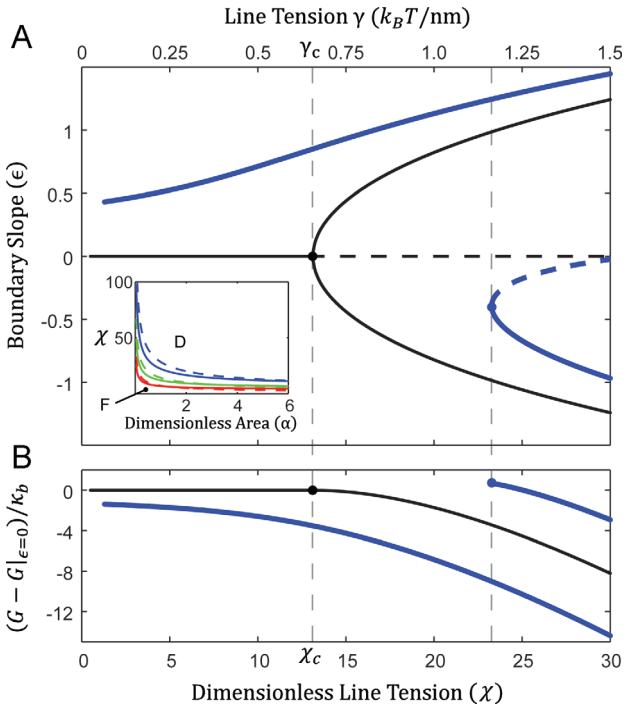

Fig. 2. Bifurcation diagram for dimpling transition at constant area (dimensionless domain area $\alpha = \pi/4$, bending modulus $\kappa_b = 25\,k_BT$, elastic decay length $\lambda_2 = 500$ nm, ratio of bending moduli $\sigma = 1$). Constant line tension and increasing area produces a qualitatively similar graph. (*A*) At zero spontaneous curvature ($\upsilon_o = 0$, thin black line) the bifurcation is symmetric, the upper and lower branches are at the same energy, and the flat domain, $\epsilon = 0$, becomes unstable above the critical point (horizontal black dashed line). With finite spontaneous curvature [$\upsilon_o = 2$, $c_o = (250\,\text{nm})^{-1}$, thick blue line] the lower energy branch (upper) has nonzero boundary slope for all line tensions, asymptoting to the zero spontaneous curvature branch. At a line tension slightly higher than the critical line tension, χ_c, for the zero spontaneous curvature case, a bifurcation yields a higher energy dimple with the opposite curvature as υ_o (indicated by the second vertical dashed line). (*Inset*) Equilibrium phase diagrams for bending moduli ratios of $\sigma = 0.5$ (red), $\sigma = 1$ (green), and $\sigma = 2$ (blue) (the dashed lines are the approximation of Eq. **8**) showing flat (F) and dimpled (D) domains. (*B*) Energy difference between the flat and dimpled state, normalized by the bending modulus κ_b, for domains with and without spontaneous curvature ($\upsilon_o = 0 \rightarrow$ thin black line; $\upsilon_o = 2 \rightarrow$ thick blue line).

space of dimensionless domain area and line tension we find the discontinuous transition (i.e., bifurcation) from a flat domain to a dimpled domain. Near the morphological transition the boundary slope grows as $|\epsilon| \propto \sqrt{\chi/\chi_c - 1}$, indicating that a dimple rapidly deviates from the flat state. The transition is symmetric, in that both possible dimple curvatures have the same energy, and hence the domain is equally likely to dimple upwards or downwards. In the experimentally relevant limit of small dimensionless domain area, the complexity of Eq. **7** is reduced to

$$\chi_c\sqrt{\alpha} = \frac{\gamma_c}{\kappa_b}\sqrt{\mathcal{A}} \simeq 8\sigma\sqrt{\pi}. \qquad [8]$$

This leads to the conclusion that the dominant parameter governing domain dimpling at zero spontaneous curvature is $\chi\sqrt{\alpha}$. For a small domain, the dimpling transition is directly regulated by domain area, the bending modulus, and line tension but only weakly depends on applied membrane tension. Intuitively, domains dimple when line tension or domain size increase, as shown in Fig. 2*A Inset*. Likewise, a decrease in bending stiffness can also induce dimpling. The effects of applied membrane tension are weak because the change in projected area upon dimpling does not lead to a significant energy cost relative to the cost of bending and line tension.

If membrane elastic properties are fixed (i.e., fixed κ_b, τ and γ), the dimpling-induced interactions "turn on" only after a critical domain size is achieved. This scenario is encountered when 2 domains, too small to dimple on their own, diffusively coalesce into a larger domain capable of dimpling and hence interacting. Indeed, such a size-selective coalescence mechanism was observed recently in model membrane vesicles (43). This constitutes a distinct class of coarsening dynamics, where classical diffusion-limited kinetics are obeyed until the domain size distribution has matured past the critical size for dimpling—then domain coalescence is a relatively slow, interaction-limited process.

For the model domain considered in Fig. 2, with area $\alpha = \pi/4$ ($r_o \simeq 250$ nm), the critical dimensionless line tension is $\chi_c \simeq 13$, corresponding to a critical line tension of $\gamma_c \simeq 0.65\,k_BT$/nm ($1\,k_BT$/nm $= 4.14$ pN). This value compares well with theoretical estimates of the line tension (28, 44) and falls squarely in the range of values from AFM measurements (2), though it is slightly higher than the value of $\gamma \simeq 0.22\,k_BT$/nm measured via shape analysis of fully phase-separated vesicles (5) and $\gamma \simeq 0.40\,k_BT$/nm measured from micropipette aspiration experiments (45). In general, measured values of the line tension depend heavily on bilayer composition, spanning a range of $\approx 0.05 - 1.5\,k_BT$/nm (2, 5, 45).

Spontaneous curvature does not affect the Euler–Lagrange equations and, hence, will not effect the class of equilibrium membrane shapes. However, domains with zero and nonzero spontaneous curvature exhibit qualitatively different behavior. Membranes can be asymmetric with respect to leaflet composition (6, 46, 47), endowing a domain with potentially large spontaneous curvature. The energetic contribution from spontaneous curvature takes the form of an additional line tension depending linearly on the slope taken by the domain boundary, ϵ. This breaks the symmetry of the membrane, giving an energetic preference to a dimple with the same curvature as the spontaneous curvature and eliminating the trivial $\epsilon = 0$ solution even at small line tensions. As line tension increases, a bifurcation produces a second, stable, higher-energy dimple of the opposite curvature as υ_o. The more energetically stable branch of this transition corresponds to a dimpled state for all values of line tension and nonzero values of domain area, as demonstrated in Fig. 2*A*. This predicts that as soon as a domain with finite spontaneous curvature forms, it dimples, regardless of size, and begins to experience interactions with any nearby dimpled domains. It is reasonable to expect that domains with similar composition will have similar spontaneous curvature, and hence form dimples whose curvature has the same sign. As we will show, dimples whose curvature has the same sign tend to interact repulsively. Such a mechanism of coalescence inhibition was observed recently in simulation (35). This indicates that control of spontaneous curvature via domain composition can regulate dimpling and hence, domain interaction (47, 48). Indeed, recent theoretical (49) work shows that lipid asymmetry leads to precisely these kinds of dimpled domains.

Calculated shapes of dimpled domains induced by line tension and spontaneous curvature are shown in Fig. 3*A*, alongside dimpled domains observed on giant unilamellar vesicles, shown in Fig. 3 *B* and *D*.

Elastic Interactions of Dimpled Domains

Given 2 domains that have met the criteria for dimpling, the deformation in the membrane surrounding the domains mediates an elastic interaction when they are within a few elastic decay lengths (λ_2) of each other. This equips us to begin addressing how small membrane domains might be achieved on short and long time scales. As previously stated, free diffusion sets the maximum rate at which a quenched membrane can evolve into a fully phase-separated membrane (23), where this evolution can happen in as little as a minute on the surface of a giant unilamellar vesicle (GUV) (3). By comparison, recycling and, hence, homogenization

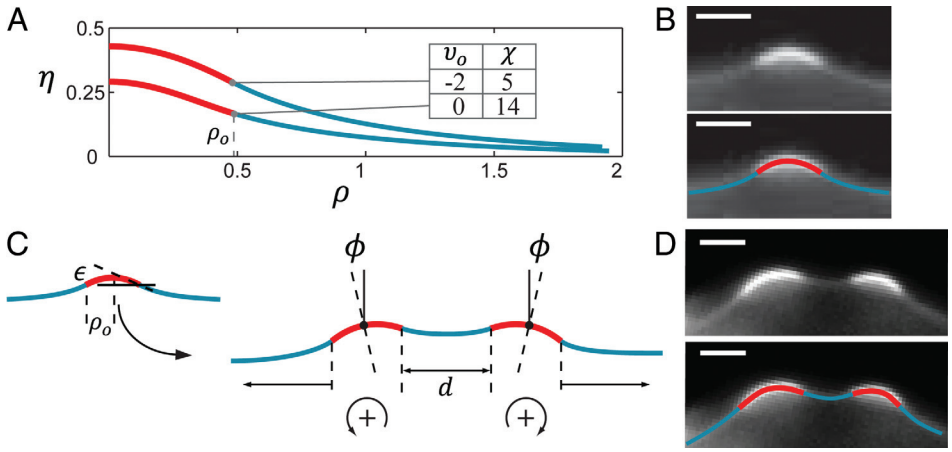

Fig. 3. Theoretical and experimental dimpled domain shapes. Domains are shown as thicker red lines, surrounding membrane as thinner blue lines. (*A*) The dimensionless height profile (η) as a function of dimensionless radius (ρ) for minimum energy dimples with and without spontaneous curvature (dimensionless spontaneous curvature, υ_o, and line tension, χ, are indicated in the legend; dimensionless domain area $\alpha = \pi/4$). (*B*) Epifluorescence cross-section of a dimple on the surface of a GUV; the red and blue lines are a guide to the eye. (*C*) 1D model of interaction—dimples maintain shape, but tilt (ϕ) as a function of separation distance (d). Dimples with the same sign of curvature repel, whereas dimples with opposite sign attract. The single domain shape, with boundary slope ϵ and dimensionless projected radius ρ_o is shown for reference. (*D*) Epifluorescence cross-section of 2 dimpled domains interacting on the surface of a GUV. (Scale bars, 3 μm.)

of cellular membrane is a process that takes place on the time scale of an hour or more (50). Our measurements of domain interactions (detailed below and other data shown in *SI Appendix*) estimate the coalescence barrier between dimpled domains at $\approx 5 - 10\, k_B T$. Hence, given the diffusion-limited rate of coalescence, interactions slow this process by approximately $e^{-5} \simeq 0.007$ to $e^{-10} \simeq 0.00005$.

The physical origin of domain interaction is explained by a simple model based on the assumption that the dimpled domain shape is constant during interaction, but the domains are free to tilt by an angle ϕ, as shown in Fig. 3*C*. This assumption was, in part, inspired by experimental observations of domain shapes on the surface of giant unilamellar vesicles, as shown, for example, in Fig. 3*D*. The interaction energy is approximately an order of magnitude less than the free energy associated with the morphological transition itself (see Fig. 2*B*), thus interaction does not perturb the domain shape significantly. Only allowing domains to rotate simplifies the interaction between 2 domains to a change in the boundary conditions in the 3 regions of interest, shown in blue in Fig. 3*C*. Applying the small gradient approximation, the boundary slope is given by $|\epsilon - \phi|$ in the outer regions and by $|\epsilon + \phi|$ in the inner region. With the single domain boundary slope, ϵ, set by the energy minimization of the previous section (i.e., eq. **6**), the pairwise energy is minimized at every domain spacing, d, by $\partial G/\partial\phi = 0$ to find the domain tilt angle that minimizes the deformation energy (see *SI Appendix* for details). This results in 2 qualitatively distinct scenarios: 2 domains whose curvatures have the same sign repel each other, whereas 2 domains whose curvatures have the opposite sign attract each other. Scaling arguments can be used to show that the strength of interaction between 2 dimpled domains increases approximately linearly with their area so long as they are both larger than some critical area (see *SI Appendix* for details). Mathematically, the assumption of rigidly rotating dimpled domains is identical to a previous 2D model of bending-mediated interactions between intramembrane proteins, represented by rigid conical inclusions (51).

Independent of the effects of spontaneous curvature, slight osmolar imbalances and constriction due to the lipid phase boundaries create small pressure gradients across the membrane that tend to orient all dimples on a vesicle in the same direction, resulting in net repulsive interactions between all domains. Transitions between "upward" and "downward" dimples are infrequent due to a large energy barrier. In the simplest case, where the domains are the same size, the tilt angle ϕ monotonically increases as 2 domains get closer, $\phi(d) \simeq -\epsilon e^{-d}$. Likewise, the interaction energy increases monotonically with decreasing domain separation, $V_{\text{int}}(d) \simeq 2\pi\kappa_b\epsilon^2\rho_o^2 e^{-d}$. To quantitatively compare our interaction model with experiment, we analyzed the thermal motion of small domains on the surface of giant unilamellar vesicles, as described in *Materials and Methods*. For direct comparison, we fit both the 1D model outlined here and the 2D inclusion model (51) to the measured potential of mean force between domains, as shown in Fig. 4. The 2 models are experimentally indistinguishable, though with a slightly different elastic decay length.

In these experiments, membrane tension was regulated by balancing the internal and external osmolarity, giving us coarse

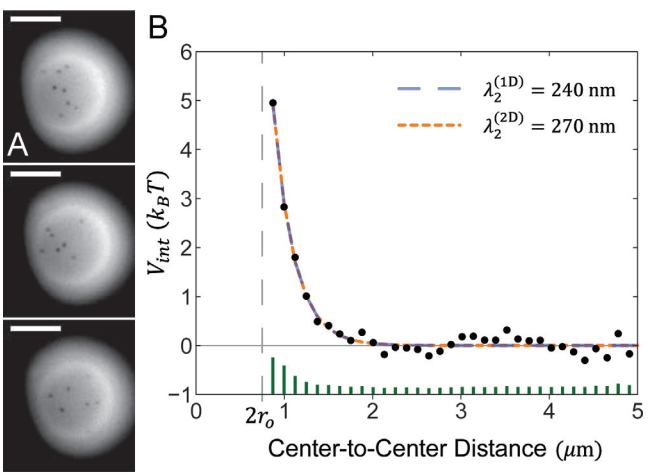

Fig. 4. Measuring domain interactions on the surface of a vesicle. (*A*) Three images of dilute interacting domains on the surface of the same vesicle. (Scale bar, 10 μm.) (*B*) The repulsive interaction potential (V_{int}) between domains on the surface of the same vesicle as *A*. The energy is measured in k_BT, and distance is domain center-to-center. The blue dashed line is a fit to the 1D interaction model in this article, $V_{\text{int}}(r) = a_1 e^{-r/\lambda_2^{(1D)}} + a_2$, with elastic decay length $\lambda_2^{(1D)} = 240$ nm. The orange dashed line is a fit to the model, $V_{\text{int}}(r) = 2\pi\kappa_b[(a_1 a_2)^2 K_0(r/\lambda_2^{(2D)}) + a_2^2 a_3^4 K_2^2(r/\lambda_2^{(2D)})] + a_4$, with elastic decay length $\lambda_2^{(2D)} = 270$ nm, based on the theory of Weikl et al. (51). Both elastic decay lengths indicate a membrane tension of $\sim 4 \times 10^{-4}\ k_BT/\text{nm}^2$. Errors bars are shown in green on the *x*-axis.

control over the elastic decay length λ_2. Through time, the distance between every domain pair was measured, and the net results were used to construct a histogram of center-to-center distance probability, the natural logarithm of which is the potential of mean force, as shown in Fig. 4*B*. We selected vesicles that had a low density of approximately equal-sized domains, and thus, generally, the interactions were described by a repulsive pairwise potential. Though areal density of domains and generic data quality varied in our experiments (see *SI Appendix*), all datasets exhibit the repulsive core of the elastic interaction. Multibody interactions occur, though infrequently; their effect can be seen as a small variation in the baseline of Fig. 4*B*, which is not captured by the pairwise interaction model. At high membrane tension, when we would not expect dimpled domains, we qualitatively verified that domains coalesce in a rapid manner as compared with our low-tension experiments (data not shown). Other recent experiments have also observed repulsive interactions and a correspondingly slower rate of coalescence between domains on low membrane tension vesicles, and a marked increase in coalescence kinetics on the surface of taut vesicles (43).

Our measurement of the pairwise potential allows us to estimate elastic properties of the membrane. The elastic decay length was fit to the 1D and 2D interaction models described above and found to be $\lambda_2^{(1D)} \simeq 240\,\text{nm}$ and $\lambda_2^{(2D)} \simeq 270\,\text{nm}$, respectively. Taken with a nominal bending modulus of $25\,k_BT$, we estimate the membrane tension to be $\approx 4 \times 10^{-4}\,k_BT/\text{nm}^2$. From the images, we measure the size of the domains at $r_o \simeq 350 - 400\,\text{nm}$, and hence $\rho_o \simeq 1.5$. We estimate the line tension, γ, using Eq. **8**, based on the fact that the domains are dimpled, and find a lower bound of $\gamma \simeq 0.49\,k_BT/\text{nm}$ ($1\,k_BT/\text{nm} = 4.14\,\text{pN}$). This is in good agreement with theoretical estimates and values determined from experiment as discussed above. Finally, viewing the repulsive core of the interaction as an effective activation barrier to coalescence, a simple Arrhenius argument suggests a decrease in coalescence kinetics by 2–3 orders of magnitude. Indeed, such a slowing of coalescence was recently observed in a similar model membrane system (43).

Discussion

Our experiments on the surface of GUVs have 3 potentially confounding effects, all due to the spherical curvature of the vesicle. First, the surface metric is not entirely flat with respect to the image plane. Thus, measurements of distance are underestimated the farther they are made from the projected vesicle center. This problem is ameliorated by concentrating on domains that are at the bottom (or top) of the vesicle where the surface is nearly flat and demanding that our tracking software exclude domains that are out of focus; see *SI Appendix* for a more detailed explanation. The second potential complication is that we use a flat 2D coordinate system for our theoretical analysis; however, domains reside on a curved surface. Given that the domain deformation, and hence energy density, decays exponentially with λ_2, as long as λ_2 is small with respect to the vesicle radius, the energetics that govern morphology converge on an essentially flat surface metric. The final complication is that the circular area of focus creates a fictitious confining potential for the domains, such that the effective measured potential of mean force is the sum of the elastic pairwise potential and a fictitious potential, $V_{\text{eff}} = V_{\text{int}} + V_{\text{fict}}$. The fictitious potential is removed by simulating noninteracting particles in a circle the same size as the radius of focus (see *SI Appendix* for details).

The constant tension ensemble used in our theoretical analysis has an experimental range of validity, determined by the excess area available on a thermally fluctuating membrane with conserved volume and total surface area $\mathcal{A}_o$ (i.e., a vesicle). In the limit where the morphological transitions use only a small portion ($\Delta\mathcal{A}$) of this excess area, defined by $k_BT/8\pi\kappa_b \gg \Delta\mathcal{A}/\mathcal{A}_o$, the tension is constant. Outside this regime, the tension rises exponentially with reduction in excess area, tending to stabilize dimples from fully budding (see *SI Appendix* for details).

In addition to the elastic mechanism of interaction, described herein, there may be other organizing forces at work in a phase-separated membrane, for instance, those of elastic (28) or entropic (52, 53) origin. However, the putative length scale over which these effects compete with thermal fluctuations (on the order of tens of nanometers) is not accessible to the spatial and temporal resolution of our experiments. Electrostatics may also be at work, in the form of dipole–dipole repulsion due to the net difference in dipole density between the 2 phases (54–56), although to first order, symmetry suggests there is a net zero dipole moment per unit volume of bilayer (57). In our experimental system, the modulator of repulsive interactions is membrane morphology (i.e., domain dimpling); if other interactions were a major repulsive effect, we would not expect such forces to depend markedly on large-scale membrane morphology.

Conclusion

We have shown that lipid domains are subject to a morphological dimpling transition that depends on the bilayer elastic properties and domain size. Dimpling allows 2 domains in proximity to repulsively interact due to the deformation in the surrounding membrane. Our model makes 2 key predictions: (*i*) at zero spontaneous curvature, the domain size distribution reaches a critical point where coalescence is arrested by repulsive interactions (43) and (*ii*) domains with finite spontaneous curvature are always subject to interaction and hence should always coalesce at a rate slower than the diffusion-limited rate (35). Additionally, the strength of elastic interactions is augmented by increasing line tension or domain area, with an approximately linear scaling. We proposed a simple 1D model of an elastic interaction that mediates dimpled-domain repulsion and then used a standard ternary membrane system to verify the existence of dimpled domains and their subsequent repulsive interaction. Our model offers a mechanism that works against diffusion-driven coalescence, to maintain small lipid domains over time.

Materials and Methods

GUVs were prepared from a mixture of DOPC (1,2-dioleoyl-sn-glycero-3-phosphocholine), DPPC (1,2-dipalmitoyl-sn-glycero-3-phosphocholine) and cholesterol (Avanti Polar Lipids, Inc.) (25:55:20/molar) that exhibits liquid–liquid phase coexistence (3). Fluorescence contrast between the 2 lipid phases is provided by the rhodamine head-group-labeled lipids: DOPE (1,2-dioleoyl-sn-glycero-3-phosphoethanolamine-*N*-(lissamine rhodamine B sulfonyl)) or DPPE (1,2-dipalmitoyl-sn-glycero-3-phosphoethanolamine-*N*-(lissamine rhodamine B sulfonyl)), at a molar fraction of ≈ 0.005. The leaflet compositions are presumed symmetric, and, hence, $\upsilon_o = 0$.

GUVs were formed via electroformation (3, 58). Briefly, 3–4 μg of lipid in chloroform were deposited on an indium–tin oxide-coated slide and dessicated for ≈ 2 h to remove excess solvent. The film was then hydrated with a 100 mM sucrose solution and heated to $\approx 50^\circ$C to be above the miscibility transition temperature. An alternating electric field was applied; 10 Hz for 120 m, 2 Hz for 50 m, at ≈ 500 Volts/m over ≈ 2 mm. Low membrane tensions were achieved by careful osmolar balancing with sucrose (≈ 100 mM) inside the vesicles, and glucose (≈ 100–108 mM) outside.

Domains were induced by a temperature quench (see *SI Appendix*) and imaged by using standard TRITC epifluorescence microscopy at 80× magnification with a cooled (-30°C) CCD camera ($6.7 \times 6.7\,\mu\text{m}^2$ per pixel, 20 MHz digitization; Roper Scientific). Images were taken from the top or bottom of a GUV where the surface metric is approximately flat (see *SI Appendix*). Datasets contained ≈ 500–$1{,}500$ frames collected at 10–20 Hz with a varying number of domains (usually 5–10). The frame rate was chosen to minimize exposure-time blurring of the domains while allowing sufficiently large diffusive domain motion. Software was written to track the position of each well-resolved domain and calculate the radial distribution function. The raw radial distribution function was corrected for the fictitious confining potential of the circular geometry (see *SI Appendix*). In the dilute interaction limit, pairwise interactions dominate, and the negative natural logarithm of the radial distribution function is the interaction potential (potential of mean force) plus a constant, as shown in Fig. 4*B*.

Note Added in Proof. Just recently, another group (59) has independently come to similar conclusions about the presence of elastically mediated interactions among dimpled domains, specifically commenting on their tendency to order domains.

ACKNOWLEDGMENTS. We thank Patricia Bassereau, Evan Evans, Ben Freund, Kerwyn Huang, Greg Huber, Sarah Keller, and Udo Seifert for stimulating discussion and comments on the manuscript and Jenny Hsaio for help with experiments. T.U. and R.P. acknowledge the support of National Science Foundation (NSF) Award CMS-0301657, NSF Award ACI-0204932, Nanoscale Interdisciplinary Research Teams Award CMS-0404031, and the National Institutes of Health Director's Pioneer Award, and National Institutes of Health Award RO1 GM084211. W.S.K. acknowledges support from NSF CAREER Award CMMI-0748034.

1. Singer SJ, Nicolson GL (1972) The fluid mosaic model of the structure of cell membranes. *Science* 175:720–731.
2. Garcia-Saez AJ, Chiantia A, Schwille P (2007) Effect of line tension on the lateral organization of lipid membranes. *J Biol Chem* 282:33537–33544.
3. Veatch SL, Keller SL (2003) Separation of liquid phases in giant vesicles of ternary mixtures of phospholipids and cholesterol. *Biophys J* 85:3074–3083.
4. Bacia K, Schwille P, Kurzchalia T (2005) Sterol structure determines the separation of phases and the curvature of the liquid-ordered phase in model membranes. *Proc Natl Acad Sci USA* 102:3272–3277.
5. Baumgart T, Hess ST, Webb WW (2003) Imaging coexisting fluid domains in biomembrane models coupling curvature and line tension. *Nature* 425:821–824.
6. Simons K, Ikonen E (1997) Functional rafts in cell membranes. *Nature* 387:569–572.
7. Sens P, Turner MS (2006) Budded membrane microdomains as tension regulators. *Phys Rev E* 73:031918.
8. Raucher D, Sheetz MP (1999) Characteristics of a membrane reservoir buffering membrane tension. *Biophys J* 77:1992–2002.
9. Simons K, Vaz WL (2004) Model systems, lipid rafts, and cell membranes. *Annu Rev Biophys Biomol Struct* 33:269–295.
10. Schlegel A, et al. (1998) Crowded little caves: Structure and function of caveolae. *Cell Signal* 10:457–463.
11. van Meer G, Sprong H (2004) Membrane lipids and vesicular traffic. *Curr Opin Cell Biol* 16:373–378.
12. Chazal N, Gerlier D (2003) Virus entry, assembly, budding, and membrane rafts. *Microbiol Mol Biol Rev* 67:226–237.
13. Mayor S, Rao M (2004) Rafts: Scale-dependent, active lipid organization at the cell surface. *Traffic* 5:231–240.
14. Dietrich C, et al. (2001) Lipid rafts reconstituted in model membranes. *Biophys J* 80:1417–1428.
15. Park H, et al. (1998) Plasma membrane cholesterol is a key molecule in shear stress-dependent activation of extracellular signal-regulated kinase. *J Biol Chem* 273:32304–32311.
16. Helms JB, Zurzolo C (2004) Lipids as targeting signals: lipid rafts and intracellular trafficking. *Traffic* 5:247–254.
17. Lucero HA, Robbins PW (2004) Lipid rafts-protein association and the regulation of protein activity. *Arch Biochem Biophys* 426:208–224.
18. Gaus K, et al. (2003) Visualizing lipid structure and raft domains in living cells with two-photon microscopy. *Proc Natl Acad Sci USA* 100:15554–15559.
19. Turner MS, Sens P, Socci ND (2005) Nonequilibrium raftlike membrane domains under continuous recycling. *Phys Rev Lett* 95:168301.
20. Gheber LA, Edidin M (1999) A model for membrane patchiness: Lateral diffusion in the presence of barriers and vesicle traffic. *Biophys J* 77:3163–3175.
21. Dietrich C, Yang B, Fujiwara T, Kusumi A, Jacobson K (2002) Relationship of lipid rafts to transient confinement zones detected by single particle tracking. *Biophys J* 82:274–284.
22. Murase K, et al. (2004) Ultrafine membrane compartments for molecular diffusion as revealed by single molecule techniques. *Biophys J* 86:4075–4093.
23. Bray AJ (2002) Theory of phase-ordering kinetics. *Adv Phys* 51:481–587.
24. Sagui S, Desai RC (1995) Ostwald ripening in systems with competing interactions. *Phys Rev Lett* 74:1119–1122.
25. Laradji M, Sunil Kumar PB (2004) Dynamics of domain growth in self-assembled fluid vesicles. *Phys Rev Lett* 93:198105.
26. Seul M, Andelman D (1995) Domain shapes and patterns: The phenomenology of modulated phases. *Science* 267:476–483.
27. Sagui C, Desai RC (1994) Kinetics of phase separation in two-dimensional systems with competing interactions. *Phys Rev E* 49:2225–2244.
28. Kuzmin PI, Akimov SA, Chizmadzhev YA, Zimmerberg J, Cohen FS (2005) Line tension and interaction energies of membrane rafts calculated from lipid splay and tilt. *Biophys J* 88:1120–1133.
29. Seul M, Morgan NY, Sire C (1994) Domain coarsening in a two-dimensional binary mixture: Growth dynamics and spatial correlations. *Phys Rev Lett* 73:2284–2287.
30. Foret L (2005) A simple mechanism of raft formation in two-component fluid membranes. *Europhys Lett* 71:508–514.
31. Harden JL, Mackintosh FC, Olmsted PD (2005) Budding and domain shape transformations in mixed lipid films and bilayer membranes. *Phys Rev E* 72:011903.
32. Taniguchi T (1996) Shape deformation and phase separation dynamics of two-component vesicles. *Phys Rev Lett*, 76:4444–4447.
33. Gozdz WT, Gompper G (2001) Shape transformations of two-component membranes under weak tension. *Europhys Lett* 55:587–593.
34. Reigada R, Buceta J, Lindenberg K (2005) Nonequilibrium patterns and shape fluctuations in reactive membranes. *Phys Rev E* 71:051906.
35. Laradji M, Kumar PB (2006) Anomalously slow domain growth in fluid membranes with asymmetric transbilayer lipid distribution. *Phys Rev E* 73:040901.
36. Freund LB, Suresh S (2004) *Thin Film Materials: Stress, Defect Formation and Surface Evolution* (Cambridge Univ Press, Cambridge, UK).
37. Boal D (2002) *Mechanics of the Cell* (Cambridge Univ Press, Cambridge UK), 1st Ed.
38. Wiggins P, Phillips R (2005) Membrane-protein interactions in mechanosensitive channels. *Biophys J* 88:880–902.
39. Helfrich W (1973) Elastic properties of lipid bilayers: theory and possible experiments. *Z Naturforsch C* 28:693–703.
40. Parthasarathy R, Yu CH, Groves JT (2006) Curvature-modulated phase separation in lipid bilayer membranes. *Langmuir* 22:5095–5099.
41. Farsad K, De Camilli P (2003) Mechanisms of membrane deformation. *Curr Opin Cell Biol* 15:372–381.
42. Rawicz W, Olbrich KC, McIntosh T, Needham D, Evans E (2000) Effect of chain length and unsaturation on elasticity of lipid bilayers. *Biophys J* 79:328–339.
43. Yanagisawa M, Imai M, Masui T, Komura S, Ohta T (2007) Growth dynamics of domains in ternary fluid vesicles. *Biophys J* 92:115–125.
44. Lipowsky R (1992) Budding of membranes induced by intramembrane domains. *J Phys II France* 2:1825–1840.
45. Tian A, Johnson C, Wang W, Baumgart T (2007) Line tension at fluid membrane domain boundaries measured by micropipette aspiration. *Phys Rev Lett* 98:208102.
46. Simons K, Ikonen E (2000) How cells handle cholesterol. *Science* 290:1721–1726.
47. Wang W, Yang L, Huang HW (2007) Evidence of cholesterol accumulated in high curvature regions: Implication to the curvature elastic energy for lipid mixtures. *Biophys J* 92:2819–2830.
48. McMahon HT, Gallop JT (2005) Membrane curvature and mechanisms of dynamic cell membrane remodelling. *Nature* 438:590–596.
49. Huang KC, Mukhopadhyay R, Wingreen NS (2006) A curvature-mediated mechanism for localization of lipids to bacterial poles. *PLoS Comput Biol* 2:e151.
50. Hansen SH, Sandvig K, van Deurs B (1992) Internalization efficiency of the transferrin receptor. *Exp Cell Res* 199:19–28.
51. Weikl TR, Kozlov MM, Helfrich W (1998) Interaction of conical membrane inclusions: Effect of lateral tension. *Phys Rev E* 57:6988–6995.
52. Dean DS, Manghi M (2006) Fluctuation-induced interactions between domains in membranes. *Phys Rev E* 74:021916.
53. Goulian M, Pincus P, Bruinsma R (1993) Long-range forces in heterogeneous fluid membranes. *Europhys Lett* 22:145–150.
54. Andelman D, Brochard F, Joanny JF (1987) Phase transitions in Langmuir monolayers of polar molecules. *J Chem Phys* 86:3673–3681.
55. McConnell HM (1989) Theory of hexagonal and stripe phases in monolayers. *Proc Natl Acad Sci USA* 86:3452–3455.
56. Liu J, Qi S, Groves JT, Chakraborty AK (2005) Phase segregation on different length scales in a model cell membrane system. *J Phys Chem B* 109:19960–19969.
57. Wohlert J, Edholm O (2004) The range and shielding of dipole–dipole interactions in phospholipid bilayers. *Biophys J* 87:2433–2445.
58. Angelova ME, Soleau S, Meleard P, Faucon JF, Bothorel P (1992) Preparation of giant vesicles by external AC electric fields. kinetics and applications. *Prog Colloid Polymer Sci* 89:127–131.
59. Semrau S, Idema T, Schmidt T, Storm C (2009) Membrane-mediated interactions measured using membrane domains. *Biophys J* 96:4906–4915.